Nontwist non-Hamiltonian systems

E. G. Altmann,* G. Cristadoro,† and D. Pazó‡
Max Planck Institute for the Physics of Complex Systems, Nöthnitzer Straße 38, 01187 Dresden, Germany
(Received 7 February 2006; published 3 May 2006)

We show that the nontwist phenomena previously observed in Hamiltonian systems exist also in time-reversible non-Hamiltonian systems. In particular, we study the two standard collision-reconnection scenarios and we compute the parameter space breakup diagram of the shearless torus. Besides the Hamiltonian routes, the breakup may occur due to the onset of attractors. We study these phenomena in coupled phase oscillators and in non-area-preserving maps.

DOI: 10.1103/PhysRevE.73.056201 PACS number(s): 05.45.Xt, 45.20.−d, 02.30.Oz

I. INTRODUCTION

Dynamical systems are usually divided into two classes, conservative and dissipative systems. Although this division is conceptually useful, it can be misleading as far as there are systems that display both dissipative and conservative (quasi-Hamiltonian) dynamics, not only for different control parameters but also coexisting in different regions of the phase space. Systems with this counterintuitive property are time reversible [1] but not Hamiltonian. Two decades ago Politi *et al.* [2] reported on a system of this type in a set of differential equations modeling a laser, and later other examples in arrays of Josephson junctions [3,4] and coupled phase oscillators [5] have been investigated.

Recently, many fundamental studies in Hamiltonian dynamics have focused on *nontwist systems*, i.e., systems where the twist condition is violated. The twist condition asserts the nondegeneracy of the frequencies in the integrable regime and it is assumed in many fundamental mathematical results [6]. In generic situations we expect it to be locally violated. In such cases it was shown that genuine nontwist phenomena appear [7,8]. More recently, it has been shown that such nontwist effects are fundamental for the understanding of many different physical systems (see Ref. [9] and references therein), e.g., the magnetic field lines in reversed shear tokamaks [9–11] and the zonal flows in geophysical fluid dynamics [12].

In this paper we provide a link between these two aspects of classical dynamics by showing that the nontwist phenomena, studied so far in Hamiltonian systems, occur also in time-reversible non-Hamiltonian systems. In particular, we show the standard collision and reconnections around the shearless torus and we study its breakup in a two-dimensional parameter space. Regarding the breakup of the shearless torus, we show that the usual Hamiltonian routes as well as a "dissipative route" exist in time-reversible non-Hamiltonian systems.

The paper is organized as follows. In Sec. II we present the definition of the twist condition and discuss the class of systems where it is expected to fail. In Secs. III and IV we present examples of the nontwist behavior in time-reversible non-Hamiltonian systems in continuous and discrete time, respectively. We summarize our conclusions in Sec. V.

II. TWIST CONDITION IN TIME-REVERSIBLE SYSTEMS

The study of near-integrable Hamiltonian systems has led to one of the greatest successes of modern classical mechanics. Near-integrable Hamiltonian systems can be written as $H(\mathbf{I},\boldsymbol{\theta})=H_0(\mathbf{I})+\epsilon H_1(\mathbf{I},\boldsymbol{\theta})$, where $(\mathbf{I},\boldsymbol{\theta})$ are the action-angle variables of the integrable Hamiltonian, H_0. In this approach, many important mathematical results [e.g., the Kolmogorov-Arnol'd-Moser (KAM) theorem] are valid assuming some nondegeneracy condition of the frequencies $\dot{\theta}_k=\partial H_0(\mathbf{I})/\partial I_k$ (see, e.g., Appendix 8 of Ref. [6]). The most common nondegeneracy condition is the twist condition, defined as

$$\det\left|\frac{\partial\dot{\theta}_k}{\partial I_j}\right|\neq 0 \quad \text{and} \quad \det\left|\frac{\partial\theta_{n+1}^{(k)}}{\partial I_n^{(j)}}\right|\neq 0 \qquad (1)$$

for continuous- and discrete-time systems, respectively. While the continuous version needs some modification when the dynamics is restricted to a specific energy shell [6], the discrete version can be directly applied to both maps and the reduced dynamics obtained by a Poincaré section of the flow. In the (near-)integrable regime the twist condition assures that the frequency of the invariant tori varies monotonically with the action. Conversely, a local violation of the twist condition usually implies the existence of a torus with maximum or minimum frequency, the so-called *shearless torus*. Around the shearless torus different *nontwist phenomena* were discovered in Hamiltonian systems, e.g., separatrix reconnections and island chain collisions [7], manifold reconnections of hyperbolic points in the chaotic regime [13], meandering [14], and the fractality of the shearless torus at criticality [8,15,16]. These phenomena were observed in area-preserving maps [7,8,17] and Hamiltonian flows with one and a half [12,18] and two [19] degrees of freedom and they typically have a strong impact in transport properties of the system.

In this paper we show the existence of the nontwist phenomena in time-reversible non-Hamiltonian maps and flows. A dynamical system is called time reversible if there is an involution G (i.e., $G^2=Id$) that reverses the direction of time. For example, for dynamical systems described by a first-order differential equation $d\mathbf{x}/dt=\mathbf{F}(\mathbf{x})$ or by a mapping $\mathbf{x}_{n+1}=L\mathbf{x}_n$ reversibility implies [1]

*Electronic address: edugalt@pks.mpg.de
†Electronic address: giampo@pks.mpg.de
‡Electronic address: pazo@pks.mpg.de

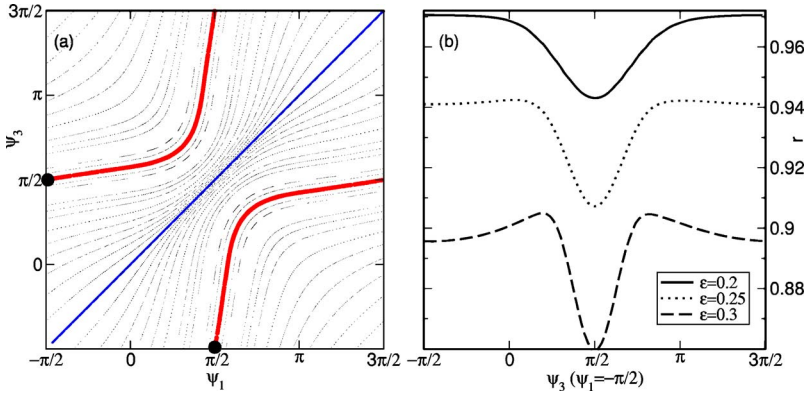

FIG. 1. (Color online) (a) Poincaré section ($\psi_2=\pi/2$) of the system in Eq. (5) for $\omega=1$, $\varepsilon=0.2$ where two nontwist tori are emphasized. IPs are marked with the symbol ●. (b) Rotation number of the tori as a function of the coordinate ψ_3 at fixed $\psi_1=-\pi/2$ for $\omega=1$ and different values of ε (see legend).

$$\frac{d(G\mathbf{x})}{dt} = -\mathbf{F}(G(\mathbf{x})) \quad \text{and} \quad L \circ G\mathbf{x}_{n+1} = G\mathbf{x}_n, \tag{2}$$

respectively. This condition alone does not ensure the observation of quasi-Hamiltonian dynamics. Additionally, the dimension of the invariant set of G should be large enough compared to the dimension D of the phase space. As discussed by Topaj and Pikovsky [5] $\dim[\mathrm{Fix}(G)] \geqslant D/2$ (D even) $[(D-1)/2$ (D odd)] is usually required for continuous systems.

The twist condition is defined for time-reversible non-Hamiltonian systems locally in the regions of the phase space where quasi-Hamiltonian dynamics is observed. Similar to the Hamiltonian case, a regime where the dynamics is locally integrable is needed in order to define action-angle variables (I,θ) to be used in Eq. (1). Many fundamental results have been obtained for the quasi-Hamiltonian dynamics of time-reversible non-Hamiltonian systems [2] (including the extension of the KAM theorem with the same optimal nondegeneracy conditions [20]), but until now there was no systematic study of the breakdown of the twist condition in these systems.

A major question in this context is in which kind of systems (Hamiltonian or time-reversible non-Hamiltonian) the violation of the twist condition is to be expected. Though we do not intend to give a general answer to this question, we note that systems possessing a symmetry in the phase space, apart from time reversibility, exhibit naturally a shearless torus. Considering that two tori related by this symmetry have the same frequency, and assuming continuity, we conclude that in the integrable limit there is at least one shearless torus between the two symmetric tori. This torus is invariant under the symmetry, what can be used (together with the involution G) to locate indicator points (IPs) [16]. IPs are points that belong to the shearless torus whenever it is not broken. Further examples are dynamical systems described by phase variables (i.e., evolving on $\mathbb{T}^D$), where the symmetry is given by the periodicity $\phi=\phi+2\pi$ of the variables. This case is exemplified in Fig. 1 for a non-Hamiltonian time-reversible system composed of phase oscillators, described by Eq. (5) below. Figure 1(a) shows that the phase space of the system is foliated by tori. Figure 1(b) shows the rotation number of these tori as a function of one phase space variable for three different control parameters ε. Due to the periodicity of the phase variables, at least two shearless torus exist (maxima and minima of the frequency). As emphasized in Fig. 1, one is located at the diagonal and the second contains the IPs $\psi_1=-\psi_3=\pm\pi/2$.

III. CONTINUOUS-TIME SYSTEMS

Time-reversible non-Hamiltonian flows are encountered in several physical situations (see [1] for a survey) such as an externally injected class-B laser [2] or arrays of N coupled differential equations [3,5]. One system where the properties discussed in Sec. II can be found is an array of N coupled phase oscillators like the one considered by Topaj and Pikovsky[5]:

$$\dot{\varphi}_k = \Omega_k + \varepsilon f(\varphi_{k-1}-\varphi_k) + \varepsilon f(\varphi_{k+1}-\varphi_k), \quad k=1,\ldots,N, \tag{3}$$

with boundary conditions $\varphi_0=\varphi_1$, $\varphi_{N+1}=\varphi_N$ and vanishing coupling when the phases of the oscillators are equal, i.e., $f(0)=0$. Taking the phase differences $\psi_k=\varphi_{k+1}-\varphi_k$ the number of variables is reduced by 1:

$$\dot{\psi}_k = \Delta_k + \varepsilon f(\psi_{k-1}) + \varepsilon f(\psi_{k+1}) - 2\varepsilon f(\psi_k), \quad k=1,\ldots,N-1 \tag{4}$$

with $\Delta_k=\Omega_{k+1}-\Omega_k$.

If f is an odd function and the natural frequencies are taken symmetrically $\Delta_k=\Delta_{N-k}$ the system is reversible. The associated involution (2) is $G:\psi_k\to\pi-\psi_{N-k}$; and $\mathrm{Fix}(G)$ is given by $\psi_k+\psi_{N-k}=\pi$. In order to visualize the nontwist phenomena mentioned in Sec. II we restrict ourselves to three variables [$N=4$ in Eq. (4)], and we analyze the dynamics by means of a two-dimensional Poincaré section at $\psi_2=\pi/2$. The set of differential equations [for concreteness we already take $f(\cdot)=\sin(\cdot)$] we will study is

$$\begin{aligned}
\dot{\psi}_1 &= \omega - 2\varepsilon\sin\psi_1 + \varepsilon\sin\psi_2,\\
\dot{\psi}_2 &= 1 - 2\varepsilon\sin\psi_2 + \varepsilon\sin\psi_1 + \varepsilon\sin\psi_3,\\
\dot{\psi}_3 &= \omega - 2\varepsilon\sin\psi_3 + \varepsilon\sin\psi_2,
\end{aligned} \tag{5}$$

where (rescaling coupling and time) we may set $\Delta_2=1$. In addition to the coupling variable ε, we take $\omega\equiv\Delta_1=\Delta_3$ as a second parameter of our system. This allows a better exploration of the behaviors of the systems (e.g., codimension-2 points); and it is also useful in order to compare our results to those obtained in the so-called standard nontwist map by two-parameter sweep [14,16].

Figure 1(a) shows a Poincaré section of the phase space for small coupling ε. Phase space is foliated by tori with

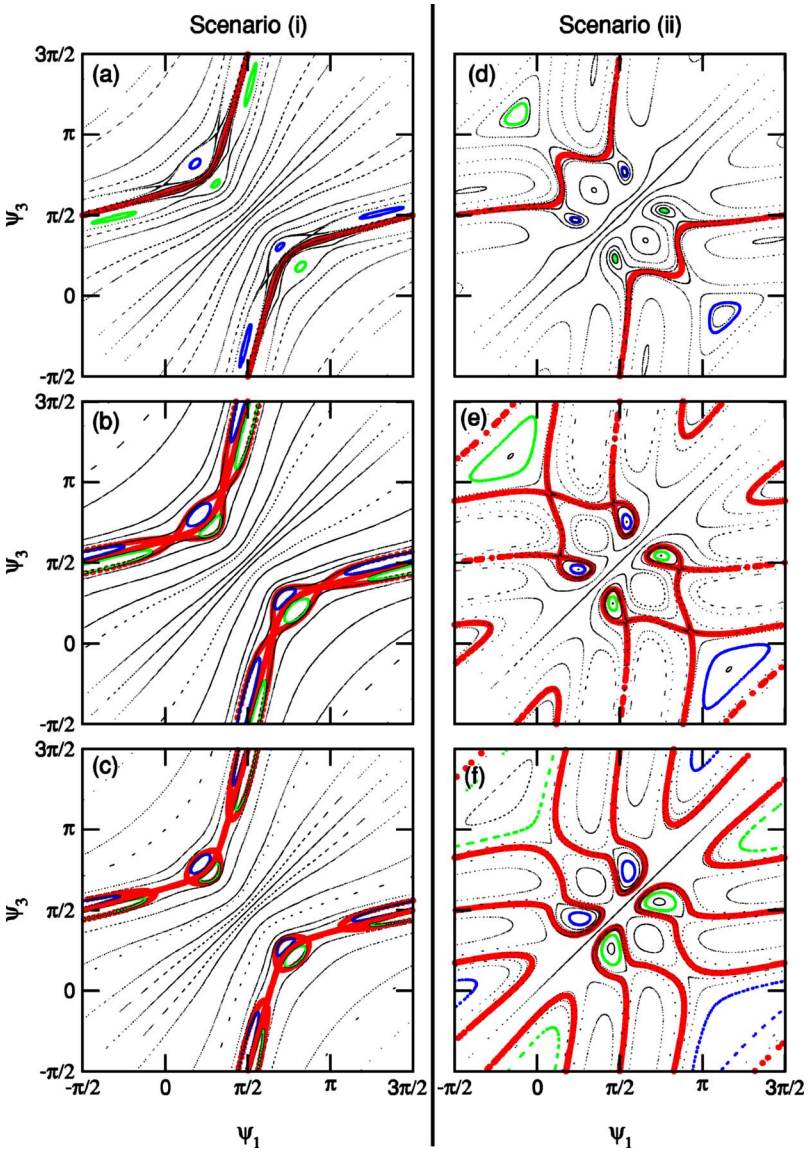

FIG. 2. (Color online) Poincaré section of system (5) for fixed $\varepsilon=0.25$ and different values of ω. Sequence (a) $\omega=0.868$, (b) $\omega=0.868\,760\,6$, and (c) $\omega=0.869$ illustrates the collision of 3:4 island chains. Sequence (d) $\omega=0.801$, (e) $\omega=0.801\,523$, and (f) $\omega=0.802$ illustrate a reconnection around 2:3 resonances.

different rotation numbers r [Fig. 1(b)]. Equation (5) is invariant under the transformation $\psi_{1,3}\rightarrow\psi_{3,1}$ which imposes the existence of the invariant manifold $\psi_1=\psi_3$ that corresponds to the diagonal shearless torus in Fig. 1. The symmetry with respect to this diagonal torus together with the involution G that maps a torus into itself allow us to locate the IPs $(\psi_1=-\psi_3=\pm\pi/2)$ for the off-diagonal shearless torus showed in Fig. 1 [we will refer to it as *the* shearless torus (ST)]. For the case $\varepsilon=0.2$ illustrated in Fig. 1(a) there are no further shearless tori. However, increasing the control parameter the rotation number of these tori may pass from maximum to minimum (or vice versa) creating other pairs of shearless tori [e.g., $\varepsilon=0.3$ shown in Fig. 1(b)]. We are specially interested in the region around the ST, where we will report in what follows the nontwist phenomena mentioned in Sec. II.

A. Collision-reconnection scenarios

We start describing the two standard collision-reconnection scenarios studied so far in nontwist Hamiltonian systems [7,30]. Figure 2 shows the two scenarios for our system: periodic orbit collision [Figs. 2(a)–2(c)] and separatrix reconnection [Figs. 2(d)–2(f)]. We find the same phenomena as in Hamiltonian systems, the only appreciable difference being the local non-volume-preservation of the flow (5). Since in the quasi-Hamiltonian dynamics the phase space volume is preserved only in time average, we see in Figs. 1(a) and 2 bunches of tori compressed and expanded in different regions of the phase space and Poincaré-Birkoff chains composed of islands of different sizes. Apart from these nonsymplectic features, Fig. 2 essentially displays the two standard scenarios.

(i) Figures 2(a)–2(c) show the collision sequence of two symmetry related Poincaré-Birkhoff chains with 3:4 rotation number, by increasing ω at fixed ε. The collision occurs in Fig. 2(b), and in Fig. 2(c) one may see the resulting dipolar structures formed by two saddle cycles on the torus and one center at each side of the ST. When ω is increased further the dipolar structure shrinks and finally disappears (at the point where the two saddle cycles on the torus annihilate each other).

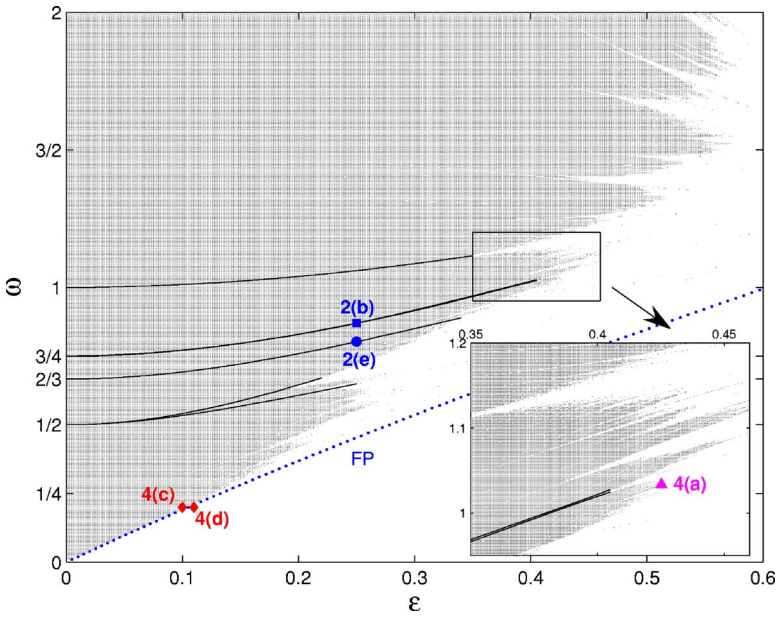

FIG. 3. (Color online) Parameter space (ε, ω) of Eq. (5). The shaded region indicates the parameters where the ST exists; the inset evidences the fractal structure of the border. Several solid lines indicate the collision-reconnection parameters for rotation numbers 1:2, 2:3, 3:4, and 1:1. The symbols (■, ●, ▲, ♦) are located at parameter values with characteristic dynamics shown in the corresponding figures. The dotted line FP marks the onset of an attracting fixed point in the system.

(ii) Figures 2(d)–2(f) show the reconnection scenario. Twin Poincaré-Birkhoff chains with 2:3 rotation number are out of phase [Fig. 2(d)] and approach each other with the ST between them. At a critical parameter [27] the separatrices of both islands reconnect [Fig. 2(e)]. Finally, past the bifurcation, the torus exhibits a characteristic meandering, due to the exchange of saddles between the two involved chains of islands.

As usually found in the literature, scenario (i) is observed for rotation numbers with even denominators, whereas scenario (ii) applies to odd denominators. Nevertheless, as demonstrated in [11], scenario (i) is not expected in the absence of symmetries [scenario (ii) is then observed for both even and odd cases] (see, e.g., [19]). As final remarks we mention that the shearless torus on the diagonal also exhibits the collision scenario [type (i)]. Heuristically the reconnection scenario [type (ii)] cannot occur because this torus is constrained to the diagonal and cannot meander. Another remark is that for resonances with small denominator (e.g., 1:1 and 1:2) a more complicated reconnection scenario occur due to the interplay of simultaneous resonances of both shearless tori (the diagonal one and the ST).

B. Destruction of the shearless torus

Our next numerical experiment was to vary the two control parameters (ε, ω), in order to find the region of parameter space where the ST exists, and in this way understand the routes for the destruction of the ST. Due to the rather difficult numerical implementation of our system (if compared to a two-dimensional map), we needed to find an efficient method to detect the existence of the ST for a large set of parameter values. By far the most efficient way we found was to resort to Slater's theorem [21]. In short, we start an initial condition at one IP and we check whether the number of different recurrence times to a small box around this point is at most 3 (see the Appendix for details).

The result of our calculation is shown in Fig. 3. The shaded region indicates the parameter values where the ST exists, while in the white zone the ST does not exist. The fractal character of the border limiting these two regions is apparent (see inset) (cf. [14,16]). The solid lines indicate the regions where a few collisions (1:2,3:4) and reconnections (2:3,1:1) occur. Regions where a couple of saddle orbits lie on the ST [as in Fig. 2(c)] are considered as regions where the ST exists (hence the shaded region between the two 1:2 lines in Fig. 3). As expected, the torus breakup is favored by the global bifurcations at the collisions and reconnections, and accordingly there is a match between the solid lines and the white "wedges" in Fig. 3. Singular points at the tips of the shaded region correspond to noble irrational rotation numbers where the torus is expected to be fractal [15,22,23]. Figures 4(a) and 4(b) show the torus just before and after destruction.

Since the system is not Hamiltonian the existence of attractors cannot be excluded [5]. For instance, below the dotted line (denoted FP line) in Fig. 3 a globally attracting fixed point exists (a periodic orbit in the full phase space). Dissipation introduces alternative ways for the destruction of the ST, as shown in Figs. 4(c) and 4(d). The bifurcation mechanism for the system (5) follows. At the FP line a marginally stable fixed point is created on the invariant set of G at $\psi_1 = \pi/2$ $(=\psi_3)$. This point belongs to the diagonal shearless torus, which is broken only through this bifurcation. Below the FP line four fixed points exist: one attractor, one repeller (mirror of the attractor as demanded by reversibility), and two saddles on the invariant set of G [see Fig. 4(d)]. Going back to the original system of $N=4$ phase oscillators, the FP line marks the onset of synchronization of oscillators 1-2, and 3-4 (i.e., a two-cluster state). Note that the usual saddle-node bifurcation in this kind of transition to synchronization is forbidden due to reversibility: for every attractor a mirror repeller must exist. In a wide region above the FP line a (chaotic) attractor and a set of Hamiltonian-like tori surrounding the diagonal torus coexist.

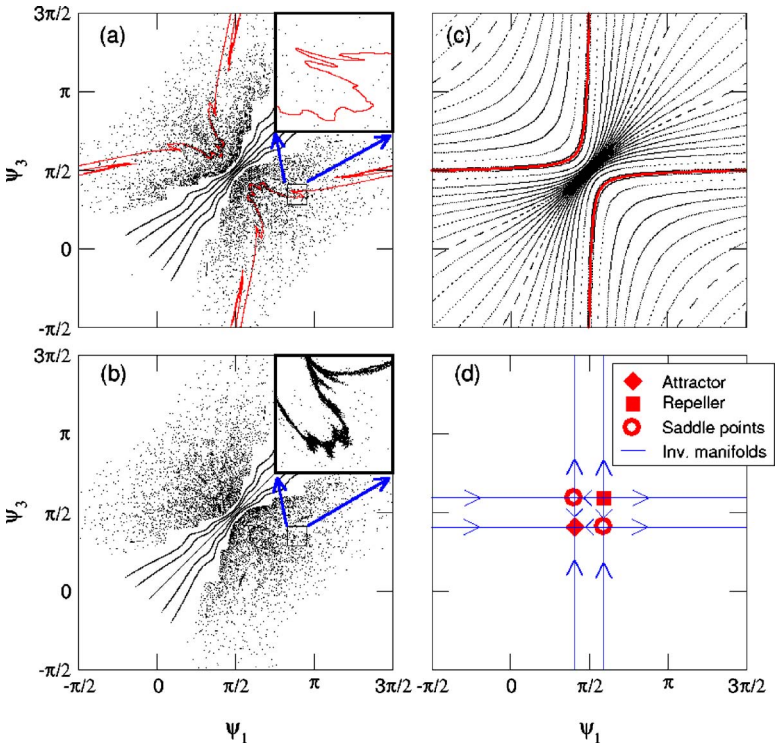

FIG. 4. (Color online) Two different routes for the breakup of the shearless torus: (a), (b) Hamiltonian-like through critical point and (c), (d) dissipative. (a) Torus near criticality $\varepsilon=0.425\,256$, $\omega=1.0335$ (the inset shows the fractal structure of the torus). (b) Torus after criticality $\varepsilon=0.425\,257$, $\omega=1.0335$ (the inset show that the torus is destroyed). (c) Near-integrable phase space $\varepsilon=0.1$, $\omega=0.2$. (d) Attracting fixed point $\varepsilon=0.11$, $\omega=0.2$.

C. Other systems

In addition to the system studied above, Eq. (5), it is interesting to mention the case of an array of N Josephson junctions subject to a parallel resistive load. This case may be described by *globally coupled* phase oscillators (see [3] where the case $N=2$ is studied in detail). For $N=3$ and assuming that two of the junctions (say $j=1$ and 3) are identical, we get a set of equations with the same symmetries as in Eq. (5):

$$\dot{\phi}_1 = \Omega + a\sin\phi_1 + \frac{1}{3}\sum_{j=1}^{3}\sin\phi_j,$$

$$\dot{\phi}_2 = \tilde{\Omega} + \tilde{a}\sin\phi_2 + \frac{1}{3}\sum_{j=1}^{3}\sin\phi_j,$$

$$\dot{\phi}_3 = \Omega + a\sin\phi_3 + \frac{1}{3}\sum_{j=1}^{3}\sin\phi_j. \tag{6}$$

We have observed in this system the same collision-reconnection scenarios described previously for system (5). As before, the diagonal torus $\phi_1=\phi_3$ ceases to exist by the onset of a stable fixed point (of the Poincaré section $\phi_2=\pi/2$). However, differently from system (5), at first this stable fixed point is not globally attracting (as in the $N=2$ case studied in [3]). Thus, the "dissipative breakup" of the off-diagonal shearless torus does not occur right after the bifurcation but only when the basin of attraction of the fixed point becomes the whole phase space.

IV. DISCRETE-TIME SYSTEMS

A simple procedure to obtain a time-reversible map is to integrate a time-reversible differential equation $\dot{\mathbf{x}}=\mathbf{F}(\mathbf{x})$ semi-implicitly [28]:

$$\mathbf{x}_{n+1}-\mathbf{x}_n = k[\mathbf{F}(\mathbf{x}_{n+1})-\mathbf{F}(\mathbf{x}_n)], \tag{7}$$

where k measures the finite-time integration step. Applying this procedure to equations of phase oscillators, similar to those studied in Sec. III, we have obtained time-reversal maps on the torus where the same nontwist phenomena were observed. Certainly, the fact that mapping (7) is defined implicitly has several drawbacks; however, avoiding details, we note that the methods to construct (explicit) time-reversal mappings described in Ref. [1] are not suited for the torus topology. In this section we study a different two-dimensional time-reversible explicit map defined on a cylinder, which illustrates that nontwist phenomena are not restricted to dynamics on a torus.

Consider the following map L:

$$y_{n+1} = \frac{y_n + a\sin(2\pi x_n)}{1+by_n\sin(2\pi x_n)},$$

$$x_{n+1} = x_n + \cos(2\pi y_{n+1}) \mod 1, \tag{8}$$

which is a particular example of a class of time-reversible maps discussed on p. 103 of Ref. [1]. Equation (8) diverges for $1+by_n\sin(2\pi x_n)=0$ and thus we restrict it to the invariant region $-\sqrt{\frac{a}{b}}<y<\sqrt{\frac{a}{b}}$ (limited by the invariant lines $y=\pm\sqrt{\frac{a}{b}}$) and the control parameters to $0\leqslant ab<1$.

The map (8) can be written as $L=M_1\circ M_2$, where $M_{1,2}$ are the following involutions:

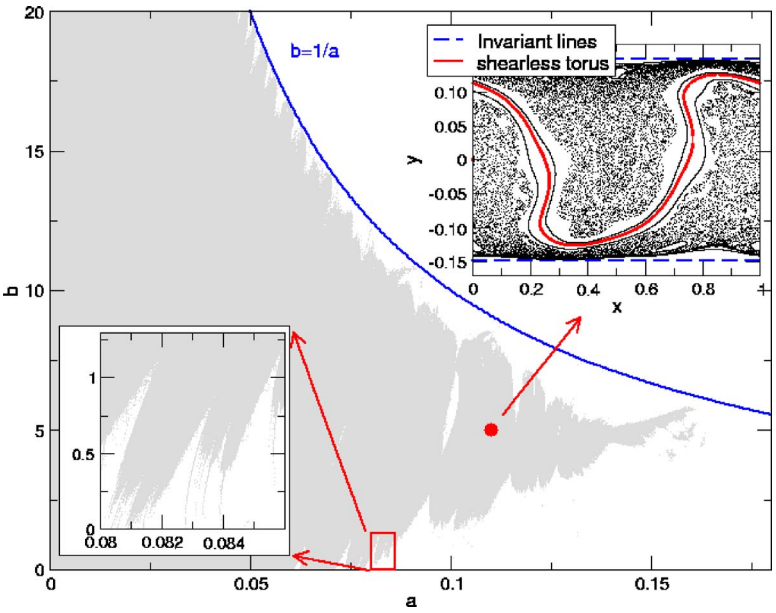

FIG. 5. (Color online) Parameter space of the map (8): shaded regions indicate the parameters where the ST exists. Above the curve $b=1/a$ the map is not defined. Lower inset: magnification showing the white wedge structure in finer scale. Upper inset: phase space for parameters $a=0.11$, $b=5$.

$$M_1: \quad x' = -x, \quad y' = \frac{y + a\sin(2\pi x)}{1 + by\sin(2\pi x)},$$

$$M_2: \quad x' = -x + \cos(2\pi y), \quad y' = y.$$

This property ensures time reversibility under $G=M_2$ [1]. The determinant of the Jacobian is given by $J=\frac{1-ab\sin^2(2\pi x)}{[1+by\sin(2\pi x)]^2}$ and shows that the map is Hamiltonian only in the case $b=0$ (when one recovers the Harper map [17]). In the limit of small control parameters the dynamics of map (8) can be considered as a perturbation of an integrable Hamiltonian system and it remains integrable almost everywhere since the KAM theorem, generalized to time-reversible systems, applies [20].

In Sec. III we argued that when at least one symmetry is present in the system, apart from time reversibility, the twist condition must be violated in the near-integrable regime. In the case of map (8) this symmetry is given by $x'=x+\frac{1}{2}, y'=-y$, which can be used (together with M_2) to determine the indicator points $x=0.25, y=0$ and $x=0.75, y=0$. According to Eq. (1) the twist condition is violated in map (8) at $y=-a\sin(2\pi x)$. In the upper inset of Fig. 5 we show the phase space of the map (8) for $a=0.11$, $b=5$. The ST intersects the curve where the twist condition is violated [8]. Using the method described in the Appendix we determined the regions of the parameter space (a,b) where this torus exists. The results are shown in Fig. 5 where a fractal-like border similar to the one observed in Fig. 3 is clearly recognizable. Indeed, we have observed numerically that all nontwist phenomena discussed in Sec. III are also observed in the time-reversible non-area-preserving map given by Eq. (8).

V. CONCLUSIONS

Time reversibility does not appear exclusively in Hamiltonian systems. Remarkably, there are time-reversible non-Hamiltonian systems that may exhibit, in addition to dynamics approaching an attractor, quasi-Hamiltonian dynamics. While major results in this context have been achieved in the past 20 years, a complete understanding of which features of Hamiltonian dynamics can be extended to reversible systems is still lacking.

Frequently, time-reversal symmetry is not the only symmetry of a system, in which case we have argued that the twist condition (i.e., the nondegeneracy of the frequencies) is violated. We have investigated the existence of nontwist phenomena, previously studied in Hamiltonian systems, in time-reversible non-Hamiltonian systems. From our results, obtained in both continuous- and discrete-time systems, we may conclude that the same nontwist phenomena are reproduced in non-Hamiltonian systems. In order to study the breakup of the shearless torus we have developed a numerical method to compute the parameter space breakup diagram (see Appendix). Our method is potentially useful in a wide class of problems concerning the detection of quasiperiodic motion in a multiparameter space. We have identified the parameter regions of the usual Hamiltonian routes of breakup of the shearless torus (through collision-reconnection and through a critical-fractal torus) and the parameters where the breakup is due to the onset of attractors.

Besides the theoretical interest of expanding the class of systems where the nontwist phenomena occur, our results are relevant for the comprehension of specific time-reversible non-Hamiltonian systems. Many dissipative systems posses an attractor of limit-cycle type where a marginally stable phase dynamics exists. The interaction of such systems may lead to quasi-Hamiltonian phase dynamics, in which case nontwist phenomena should be expected. Usually a large number of oscillators are coupled, what provides additional motivation for the extension of the nontwist phenomenology to higher dimensions [31]. Indeed conservative dynamics has been already observed in phase models such as the dynamics of solitary waves in chains of dispersively coupled oscillators [24], and the finite-dimensional Kuramoto model [25]. The role of time reversibility and the violation of the twist condition in these non-Hamiltonian models remains to be understood.

ACKNOWLEDGMENTS

We thank R. D. Vilela and J. S. E. Portela for a careful reading of the manuscript. E.G.A. was supported by CAPES (Brazil).

APPENDIX

The knowledge of the critical parameter values of a map where an invariant rotational circle breaks can be crucial in many situations. We briefly describe here the techniques previously employed to calculate the breakup diagram of the shearless torus and we introduce a method that has proven to be computationally efficient. Even though we have applied our method to compute the breakup diagram it is rather general and we believe that it can be useful whenever quasiperiodic motion has to be efficiently detected.

The first breakup diagrams were calculated [16] considering the torus to be destroyed whenever a trajectory started at an IP leaves a region that certainly would contain the curve. A slightly different method was proposed in Ref. [14] using the fact that a trajectory in a periodic or quasiperiodic motion leads to a converging winding number. These procedures can be computationally expensive: in a typical mixed phase space we expect that a trajectory will stick around the complex structure of cantori and regular islands while wandering into the chaotic sea and the time needed to detect the nonexistence of the tori could be very large. A refined method relies on Greene's residue criterion and can be used when high accuracy is needed (e.g., to precisely locate critical points in the breakup diagram corresponding to noble rotation numbers) while it is not suited to explore a large parameter region [8,22].

Here we take advantage of a simple property of rotations in one dimension to develop a method that is together fast and quite robust, and hence suited to scan a large set of parameters. The quasiperiodic dynamics restricted to the torus can be reduced to a simple rotation of the circle using a natural parametrization of the curve (an example can be found in [26]). Slater's theorem [21] states that for any irrational rotation ω and for any connected interval there are at most three different return times. Moreover, in the case of three different return times one of them is the sum of the other two and two of them are always consecutive denominators in the continued fraction expansion of the irrational number ω.

Accordingly, our method simply consists in counting the number of different return times of the iterates of the IP x_0 inside an arbitrary region that contains a connected part of the torus around x_0 (for the specific cases Figs. 3 and 5 we used a box centered at one IP [29]). The torus is considered to be broken whenever the different return times violate the conditions imposed by Slater's theorem (e.g., whenever their number exceeds 3). When the rotation number of the torus is not known *a priori* (as in our case) the additional restriction that uses its continued fraction expansion cannot be used.

The implementation of the procedure is straightforward provided one point on the torus is known (IP). It is evident that the constraints on the return times are quite restrictive and they are typically rapidly failing when the torus is broken and the trajectory enters the chaotic sea.

[1] J. A. G. Roberts and G. R. W. Quispel, Phys. Rep. **216**, 63 (1992).
[2] A. Politi, G. L. Oppo, and R. Badii, Phys. Rev. A **33**, 4055 (1986).
[3] K. Y. Tsang, R. E. Mirollo, S. H. Strogatz, and K. Wiesenfeld, Physica D **48**, 102 (1991).
[4] K. Y. Tsang, S. H. Strogatz, and K. Wiesenfeld, Phys. Rev. Lett. **66**, 1094 (1991).
[5] D. Topaj and A. Pikovsky, Physica D **170**, 118 (2002).
[6] V. Arnold, *Mathematical Methods of Classical Mechanics* (Springer, New York, 1978).
[7] J. E. Howard and S. M. Hohs, Phys. Rev. A **29**, 418 (1984); J. E. Howard and J. Humpherys, Physica D **80**, 256 (1995).
[8] D. del Castillo-Negrete, J. M. Greene, and P. J. Morrison, Physica D **91**, 1 (1996).
[9] P. Morrison, Phys. Plasmas **7**, 2279 (2000).
[10] R. Balescu, Phys. Rev. E **58**, 3781 (1998); W. Horton *et al.*, Phys. Plasmas **5**, 3910 (1998); M. Roberto, E. C. da Silva, I. L. Caldas, and R. Viana, *ibid.* **11**, 214 (2004).
[11] E. Petrisor, J. H. Misguich, and D. Constaniescu, Chaos, Solitons Fractals **18**, 1085 (2003).
[12] D. del Castillo-Negrete and P. J. Morrison, Phys. Fluids A **5**, 948 (1993).
[13] G. Corso and F. B. Rizzato, Phys. Rev. E **58**, 8013 (1998).
[14] A. Wurm, A. Apte, K. Fuchss, and P. Morrison, Chaos **15**, 023108 (2005).
[15] D. del Castillo-Negrete, J. M. Greene, and P. J. Morrison, Physica D **100**, 311 (1997).
[16] S. Shinohara and Y. Aizawa, Prog. Theor. Phys. **97**, 379 (1997); **100**, 219 (1998).
[17] S. Saitô, Y. Nomura, K. Hirose, and Y. Ichikawa, Chaos **7**, 245 (1997).
[18] E. Shuckburgh and P. Haynes, Phys. Fluids **15**, 3342 (2003).
[19] G. Stagika and S. Ichtiaroglou, Celest. Mech. Dyn. Astron. **78**, 151 (2000).
[20] M. B. Sevryuk, Physica D **112**, 132 (1998).
[21] N. Slater, Proc. Cambridge Philos. Soc. **63**, 1115 (1967).
[22] A. Apte, A. Wurm, and P. Morrison, Chaos **13**, 421 (2003).
[23] D. Gaidashev and H. Koch, Nonlinearity **17**, 1713 (2004).
[24] P. Rosenau and A. Pikovsky, Phys. Rev. Lett. **94**, 174102 (2005).
[25] O. V. Popovych, Y. L. Maistrenko, and P. A. Tass, Phys. Rev. E **71**, 065201 (2005).
[26] A. Apte, R. de la Llave, and N. Petrov, Nonlinearity **18**, 1173 (2005).
[27] Actually, the reconnection will not occur exactly in a line in the two-parameter space but in a (very) thin region as discussed by A. Apte, R. de la Llave, and E. Petrisor, Chaos, Solitons Fractals **27**, 1115 (2006).
[28] A. Pikovsky (private communication).

[29] The shearless torus near criticality is strongly meandering and some care in the choice of the recurrence region has to be taken in order to avoid the torus multiply crossing it.

[30] A dissipative analogous of these reconnections switches the basins of attraction of two stable foci. See, e.g., J. P. Van der Weele and T. P. Valkering, Physica A **169** 42 (1990); S. M. Soskin *et al.*, Phys. Rep. **373** 247 (2003).

[31] Examples of nontwist singularities for high-dimensional sympletic maps are extensively studied in H. R. Dullin and J. D. Meiss, Chaos **13** 1 (2003).